# Cationic Iridium(III) Complexes with Two Carbene-Based Cyclometalating Ligands: Cis Versus Trans Isomers

Filippo Monti,*[†,‡] Maria Grazia I. La Placa,[†] Nicola Armaroli,*[†] Rosario Scopelliti,[§] Michael Grätzel,[§] Mohammad Khaja Nazeeruddin,[§] and Florian Kessler*[§,⊥]

[†]Istituto per la Sintesi Organica e la Fotoreattività, Consiglio Nazionale delle Ricerche, Via P. Gobetti 101, 40129 Bologna, Italy
[‡]Dipartimento di Chimica "G. Ciamician", Università di Bologna, Via F. Selmi 2, 40126 Bologna, Italy
[§]Laboratory of Photonics and Interfaces, Institute of Chemical Sciences and Engineering, École Polytechnique Fédérale de Lausanne, CH-1015 Lausanne, Switzerland

S *Supporting Information*

ABSTRACT: A series of cationic iridium(III) complexes with two carbene-based cyclometalating ligands and five different N^N bipyridine and 1,10-phenanthroline ancillary ligands is presented. For the first time—in the frame of a rarely studied class of bis(heteroleptic) iridium complexes with two carbene-based cyclometalating ligands—a pair of cis and trans isomers has been isolated. All complexes (*trans*-**1**−**5** and *cis*-**3**) were characterized by ^{1}H NMR, ^{13}C NMR, ^{31}P NMR, and HRMS (ESI-TOF); in addition, crystal structures of *cis*-**3** and *trans*-**4** are reported and discussed. Cyclic voltammetric studies show that the whole series exhibits highly reversible oxidation and reduction processes, suggesting promising potential for optoelectronic applications. Ground-state DFT and TD-DFT calculations nicely predict the blue shift experimentally observed in the room-temperature absorption and emission spectra of *cis*-**3**, compared to the trans complexes. In CH$_3$CN, *cis*-**3** displays a 4-fold increase in photoluminescence quantum yield (PLQY) with respect to *trans*-**3**, as a consequence of drastically slower nonradiative rate constant. By contrast, at 77 K, the emission properties of all the compounds, including the cis isomer, are much more similar, with a pronounced hypsochromic shift for the trans complexes. A similar behavior is found in solid state (1% w/w poly(methyl methacrylate) matrix), with all complexes displaying PLQY of ~70−80%, comparable emission lifetimes ($\tau \approx 1.3$ μs), and a remarkable rigidochromic shift. To rationalize the more pronounced nonradiative deactivation (and smaller PLQY) observed for photoexcited trans complexes, comparative temperature-dependent emission studies in the range of 77−450 K for *cis*-**3** and *trans*-**3** were made in propylene glycol, showing that solvation effects are primarily responsible for the observed behavior.
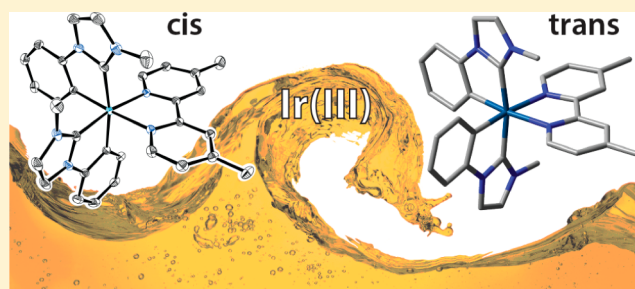
INTRODUCTION

Neutral and cationic luminescent cyclometalated iridium(III) complexes have attracted a great deal of attention in recent years.[1,2] They have found many applications such as organic light-emitting diodes (OLEDs),[3−6] light-emitting electrochemical cells (LECs),[7−10] water splitting,[11,12] oxygen sensors,[13] protein staining,[14] biolabeling,[15] sensing of biological metal ions,[16] and cell imaging.[17] They are termed homoleptic when three identical chelating ligands make up the octahedral coordination environment, bis(heteroleptic) when two identical main ligands and one so-called ancillary ligand are present, and tris(heteroleptic) when the three ligands around the Ir(III) center are different. The latter are rather challenging to make and appeared only recently in the literature,[18] whereas homoleptic complexes are easily accessible and have been widely studied.[2] On the other hand, bis(heteroleptic) complexes are relatively easy to make through the preparation of a stable chloro-bridged iridium intermediate with general formula [(C^N)$_2$Ir(μ-Cl)]$_2$, where C^N is a bidentate

cyclometalating ligand such as phenyl-pyridine. Eventually, the dimer can be reacted with a negatively charged bidentate ligand (e.g., picolinate) to form a neutral complex or with a neutral bidentate chelator (e.g., bipyridine) to form a cationic iridium complex;[19] the photophysical and electrochemical properties of such complexes can be widely tuned by ligand design.[7,20,21] The nitrogen donor atoms of the C^N ligands of the dimer are usually in trans orientation to each other,[22] and only recently the groups of De Cola[23] and Bryce[24] reported independently two rare examples of cis orientation of the nitrogen atoms to each other. The trans orientation also typically occurs with C^C: cyclometalating ligands, where C: indicates a carbene-type carbon atom.[25] Many carbene-containing cyclometalating iridium complexes have been reported, but the largest majority are homoleptic or bis-(heteroleptic) complexes of [Ir(:C^C)$_3$] general structure[25−28]

and $[Ir(C^\wedge N)_2(:C^\wedge X)]$ (X = N or :C), where in the latter the carbene-type chelators are normally the ancillary ligands.[29−31] Bis(heteroleptic) Ir(III) complexes containing two carbene main ligands remain scarce, and observation of cis and trans isomers has never been reported for this class of compounds, to the best of our knowledge.[17,32−35]

In this work, we present a series of cationic iridium(III) complexes with two carbene-based cyclometalating ligands and five different N^N ancillary ligands based on bipyridine and 1,10-phenanthroline. In addition to the typical trans complexes, in one case we were also able to isolate and characterize the cis isomer. We report herein an extensive investigation of the structural, electrochemical, and photophysical properties of these novel compounds, also supported by density functional theory (DFT) calculations. A systematic comparison of the trans and cis isomer pair evidences remarkable differences of the photophysical properties, which were rationalized also with the support of temperature-dependent photophysical studies.

■ EXPERIMENTAL PROCEDURES

Materials and Methods. $[Ir(cod)(\mu\text{-}Cl)]_2$ was purchased from MCAT (Germany) and 1-phenylimidazole was purchased from Fluorochem. All solvents were use as p.a. grade and degassed by six consecutive vacuum and backfill cycles. All other materials and solvents were of reagent quality and used as received. ^1H and ^{13}C NMR spectra were recorded using a Bruker AV 400 MHz spectrometer. Chemical shifts δ (in ppm) are referenced to residual solvent peaks. For ^1H NMR: CDCl₃, 7.26 ppm; for ^{13}C NMR: CDCl₃, 77.0 ppm. ^{31}P NMR spectra were recorded using a Bruker AVANCEIII 400 MHz spectrometer. Coupling constants are expressed in hertz (Hz). High-resolution mass spectra (HRMS) were obtained with a Waters Q-TOF-MS instrument using electrospray ionization (ESI). The diffraction data of compounds **cis-3** and **trans-4** were obtained at low temperature [100(2) K] using Mo Kα radiation on a Bruker APEX II CCD diffractometer equipped with a κ geometry goniometer. The data sets were reduced by EvalCCD[36] and then corrected for absorption.[37] The solutions and refinements were performed by SHELX.[38] The crystal structures were refined using full-matrix least-squares based on F^2 with all non-hydrogen atoms anisotropically defined. Hydrogen atoms were placed in calculated positions by means of the "riding" model. Some PF_6 anions showed extensive disordering, and their refinement was handled by the split model in combination with some suitable restraints (SIMU and SADI cards). Additional electron density (corresponding to disordered solvent molecules), found in the difference Fourier map of complex **trans-4**, was treated by the SQUEEZE algorithm of PLATON.[39]

Electrochemistry. Voltammetric measurements were made with a personal computer-controlled AutoLab PSTAT10 electrochemical workstation. Solutions were degassed by bubbling argon for 20 min. Cyclic voltammograms (CV) were obtained at a scan rate of 50 mV/s using 0.1 M $TBAPF_6$ as supporting electrolyte in acetonitrile (CH₃CN). Glassy carbon, platinum plate, and platinum wire were employed as working, counter, and reference electrodes, respectively. At the end of each measurement, ferrocene was added as internal reference.

Computational Details. DFT calculations were carried out with the D.01 revision of the Gaussian 09 program package,[40] using the PBE0 hybrid functional[41,42] and the 6-31G(d,p) basis set for C, H, and N atoms;[43] the "double-ζ" quality LANL2DZ basis set was selected as pseudopotential for the Ir metal center.[44] The **trans-3−4** and **cis-3** complexes were fully optimized in acetonitrile without imposing any symmetry constraints both in the electronic ground state and in the lowest triplet state, by using the polarizable continuum model (PCM).[45−47] A frequency calculation was always used to confirm that the stationary point found by the geometry optimization was actually corresponding to a minimum on the potential energy surface (no imaginary frequencies). Time-dependent (TD) DFT calcula-

tions,[48−50] at the same level of theory used for geometrical optimization, were employed to simulate the absorption spectra of all the molecules in their optimized ground-state geometry (S_0). The first 100 singlet and 12 triplet vertical excitations were computed for the complexes. To investigate the nature of the lowest triplet excited state (T_1), geometry optimizations and related frequency calculations were performed at the spin-unrestricted UPBE0 level of theory, imposing a spin multiplicity of three. The emission energy from the lowest triplet excited state was estimated by subtracting the self-consistent field energy of the T_1 state in its minimum conformation from that of the singlet ground state having the same geometry of T_1. All the pictures of molecular orbitals and spin-density surfaces were created using GaussView 5 for Mac.[51]

Photophysical Measurements. The spectroscopic investigations were performed in spectrofluorimetric grade CH₃CN and CH₂Cl₂. The absorption spectra were recorded with a PerkinElmer Lambda 950 spectrophotometer. For the photoluminescence experiments, the samples were placed in fluorimetric Suprasil quartz cuvettes (1 cm) and purged of oxygen by bubbling argon. The uncorrected emission spectra were obtained with an Edinburgh Instruments FLS920 spectrometer equipped with a Peltier-cooled Hamamatsu R928 photomultiplier tube (PMT) (185−850 nm). An Edinburgh Xe 900 with 450 W xenon arc lamp was used as the excitation light source. The corrected spectra were obtained via a calibration curve supplied with the instrument. The luminescence quantum yields (Φ_{PL}) in solution were obtained from the corrected spectra on a wavelength scale (nm) and measured according to the approach described by Würth et al.,[52] using an air-equilibrated water solution of $[Ru(bpy)_3]$-Cl_2 as reference ($\Phi_L = 0.028$)[53] as standard. The emission lifetimes (τ) in the nanosecond and microsecond ranges were measured through the time-correlated single photon counting (TCSPC) technique with the use of the same luminescence spectrometer described above and equipped with a laser diode as the excitation source (1 MHz; λ_{exc} = 407 nm; 200 ps time resolution after deconvolution) and the aforementioned PMT as detector. The analysis of the luminescence decay profiles was accomplished with the software provided by the manufacturer, and the quality of the fit was assessed with the χ^2 value close to unity and with the residuals regularly distributed along the time axis. To record the 77 K luminescence spectra, samples were put in quartz tubes (2 mm inner diameter) and inserted into a special quartz Dewar flask filled with liquid nitrogen. Solid samples were prepared following two different procedures: the poly(methyl methacrylate) (PMMA) films containing 1 wt % of the complex were drop-cast from dichloromethane solutions; the neat films of the complexes were spin coated from acetonitrile solutions. The thickness of the films was not controlled. Solid-state Φ_{PL} values were calculated by corrected emission spectra obtained from an Edinburgh FLS920 spectrometer equipped with a barium sulfate-coated integrating sphere (diameter of 4 in.) following the procedure described by De Mello et al. .[54] Experimental uncertainties are estimated to be ±8% for τ determinations, ±20% for Φ_{PL}, and ±2 nm and ±5 nm for absorption and emission peaks, respectively.
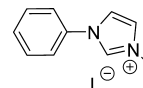

3-Methyl-1-phenyl-1H-imidazol-3-ium iodide. 1-Phenylimidazole (3.1 g, 21.4 mmol, 1 equiv) was put into a flask under nitrogen. Then 10 mL of dry toluene and 2.7 mL (42.8 mmol, 2 equiv) of MeI were added via syringe. The mixture was heated to 50 °C for 4 h. Then the precipitate was collected and washed with toluene to obtain 7.75 g (28.9 mmol, 92%) of the pure product as white solid. The observed chemical shifts in the proton NMR spectra correspond well to those reported in literature.[17]

[Ir(Ph-Im)₂(μ-Cl)]₂. 2.69 g (4.0 mmol, 1 equiv) of $[Ir(COD)(\mu\text{-}Cl)]_2$, 2.02 g (8.8 mmol, 2.2 equiv) of Ag₂O, and 2.52 g (8.8 mmol, 2.2 equiv) of 3-methyl-1-phenyl-1H-imidazol-3-ium iodide were put into a two-neck round-bottom flask equipped with a reflux condenser. 1,2-Dichloroethane (200 mL) was added under nitrogen, and the solution

trans-1
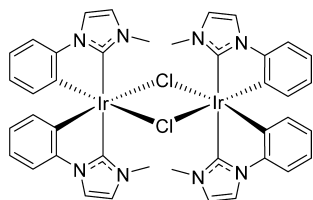
was degassed by six vacuum and backfill cycles. The mixture was heated to reflux overnight. After it cooled to room temperature, the solution was filtered through Celite to remove silver residues, and the Celite was washed with CH_2Cl_2. The orange solution was concentrated and dried in vacuo to obtain the crude product as brown solid in quantitative yield (3.65 g, 4.0 mmol). The crude was used without further purification.
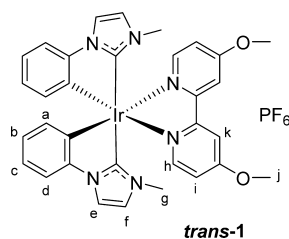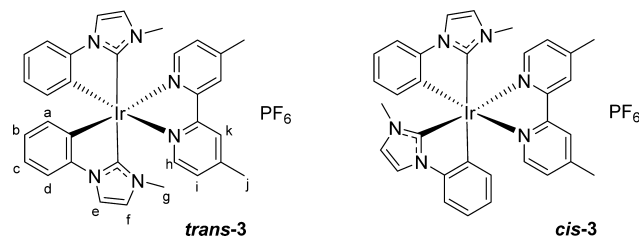
trans-1. A solution of 259 mg (1.2 mmol, 3 equiv) of 4,4′-dimethoxy-2,2′-bipyridine and 356 mg (0.4 mmol, 1 equiv) of $[\mathbf{Ir(Ph\text{-}Im)_2(\mu\text{-}Cl)}]_2$ in 20 mL of CH_2Cl_2 was stirred overnight under nitrogen at room temperature. Then the dark solution was concentrated, and the crude product was prepurified on a short plug of silica gel using 2% of acetone in CH_2Cl_2 as solvent. After impurities were removed, KPF_6 in acetone was used as the eluent to elute the product as the corresponding PF_6 salt. The solvent was removed in vacuo, and the solid was redissolved in CH_2Cl_2 and filtered through cotton to remove excess of KPF_6. The product was purified on silica gel using CH_2Cl_2 and then 2% of acetone in CH_2Cl_2 as solvent. 89 mg (0.10 mmol, 13% yield based on $[\mathbf{Ir(Ph\text{-}Im)_2(\mu\text{-}Cl)}]_2$) of the pure product was obtained as yellow solid. ^{1}H NMR (400 MHz, CDCl3): δ 7.98 (d, [3]J_{HH} = 2.6 Hz, 2H, H$_h$), 7.83 (d, [3]J_{HH} = 6.4 Hz, 2H, H$_a$), 7.47 (d, [4]J_{HH} = 2.1 Hz, 2H, H$_k$), 7.15 (dd, [3]J_{HH} = 7.8 Hz, [4]J_{HH} = 1.2 Hz, 2H, H$_c$), 6.96 (td, [3]J_{HH} = 7.6 Hz, [4]J_{HH} = 1.4 Hz, 2H, H$_b$), 6.91 (d, [4]J_{HH} = 2.0 Hz, 2H, H$_d$), 6.81 (dd, [3]J_{HH} = 6.4 Hz, [4]J_{HH} = 2.6 Hz, 2H, H$_i$), 6.73 (td, [3]J_{HH} = 7.4 Hz, [4]J_{HH} = 1.3 Hz, 2H, H$_e$), 6.44 (dd, [3]J_{HH} = 7.4 Hz, [4]J_{HH} = 1.3 Hz, 2H, H$_f$), 4.13 (s, 6H, H$_j$) 3.08 (s, 6H, H$_g$) ppm. ^{13}C NMR (100 MHz, CDCl3): δ 171.0 (NCN), 167.2, 158.2, 151.2, 146.5, 137.5, 134.0, 126.1, 122.2, 122.0, 115.4, 114.9, 111.6, 109.3 (ArC), 56.8 (OCH_3), 35.4 (NCH_3) ppm. ^{31}P NMR (81 MHz, CDCl3): δ −144.4 (sept, [1]J_{PF} = 713 Hz, PF_6) ppm. HRMS (ESI-TOF) m/z (%): calcd. 723.2061; found 723.2047 (100) $[(M − PF_6)^+]$.
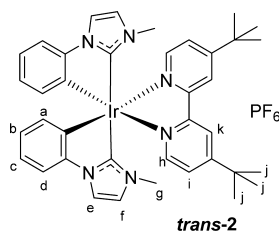
trans-2

trans-2. A solution of 357 mg (1.33 mmol, 3.3 equiv) of 4,4′-di-*tert*-butyl-2,2′-bipyridine and 356 mg (0.4 mmol, 1 equiv) of $[\mathbf{Ir(Ph\text{-}Im)_2(\mu\text{-}Cl)}]_2$ in 20 mL of CH_2Cl_2 was stirred overnight under nitrogen at room temperature. Then the dark solution was concentrated, and the crude product was prepurified on a short plug of silica gel using 2% of acetone in CH_2Cl_2 as solvent. After removing impurities, KPF_6 in acetone was used as the eluent to elute the product as the corresponding PF_6 salt. The solvent was removed in vacuo, and the solid was redissolved in CH_2Cl_2 and filtered through cotton to remove excess of KPF_6. The product was purified on silica gel using

2% of acetone in CH_2Cl_2 as solvent. 99 mg (0.11 mmol, 13% yield based on $[\mathbf{Ir(Ph\text{-}Im)_2(\mu\text{-}Cl)}]_2$) of the pure product was obtained as yellow solid. ^{1}H NMR (400 MHz, CDCl3): δ 8.33 (d, [3]J_{HH} = 1.8 Hz, 2H, H$_k$), 8.02 (d, [3]J_{HH} = 6.0 Hz, 2H, H$_h$), 7.46 (d, [4]J_{HH} = 2.1 Hz, 2H, H$_a$), 7.33 (dd, [3]J_{HH} = 5.9 Hz, [4]J_{HH} = 2.0 Hz, 2H, H$_i$), 7.15 (dd, [3]J_{HH} = 7.8 Hz, [4]J_{HH} = 1.1 Hz, 2H, H$_c$), 6.98 (td, [3]J_{HH} = 7.6 Hz, [4]J_{HH} = 1.4 Hz, 2H, H$_b$), 6.95 (d, [4]J_{HH} = 2.0 Hz, 2H, H$_d$), 6.75 (td, [3]J_{HH} = 7.4 Hz, [4]J_{HH} = 1.3 Hz, 2H, H$_e$), 6.45 (dd, [3]J_{HH} = 7.4 Hz, [4]J_{HH} = 1.3 Hz, 2H, H$_f$), 3.03 (s, 6H, H$_g$) 1.45 (s, 18H, H$_j$) ppm. ^{13}C NMR (100 MHz, CDCl3): δ 170.3 (NCN), 162.9, 156.3, 150.6, 146.4, 137.4, 133.9, 126.2, 124.8, 122.3, 122.3, 120.9, 114.9, 111.6 (ArC), 35.6 (NCH_3), 35.2 (C(CH3)3) 30.3 (C(CH_3)3) ppm. ^{31}P NMR (81 MHz, CDCl3): δ −144.5 (sept, [1]J_{PF} = 713 Hz, PF_6) ppm. HRMS (ESI-TOF) m/z (%): calcd. 775.3102; found 775.3092 (100) $[(M − PF_6)^+]$.

trans-3 *cis-3*

trans-3 and cis-3. A solution of 111 mg (0.6 mmol, 1 equiv) of 4,4′-dimethyl-2,2′-bipyridine and 356 mg (0.4 mmol, 1.33 equiv) of $[\mathbf{Ir(Ph\text{-}Im)_2(\mu\text{-}Cl)}]_2$ in 20 mL of CH_2Cl_2 was stirred overnight under nitrogen at room temperature. Then the dark solution was concentrated, and the crude product was purified by column chromatography on silica gel using 2% of acetone in CH_2Cl_2 as solvent mixture to remove impurities. Then KPF_6 was added to the solvent mixture to elute the product from the silica as the corresponding PF_6 salt of the complex. First pure **trans-3** was eluted as yellow solution (orange emitting under UV light, R_f = 0.63−0.73 in CH_2Cl_2/acetone = 4/1), and then small quantities of **cis-3** were eluted as pale yellow solution (yellow emitting under UV light, R_f = 0.38−0.48 in CH_2Cl_2/acetone = 4/1). Then **cis-3** was dissolved in CH_2Cl_2 filled in a crystallization tube, and a layer of heptane was added on top. Single crystals suitable for X-ray structure analysis were obtained from this solution.

trans-3. 101 mg (0.12 mmol, 20% yield based on 4,4′-dimethyl-2,2′-bipyridine) of pure **trans-3** were obtained as orange solid. ^{1}H NMR (400 MHz, CDCl3): δ 8.47 (s, 2H, H$_k$), 7.92 (d, [3]J_{HH} = 5.6 Hz, 2H, H$_h$), 7.47 (d, [3]J_{HH} = 2.0 Hz, 2H, H$_a$), 7.16 (dd, [3]J_{HH} = 7.8 Hz, [4]J_{HH} = 1.0 Hz, 2H, H$_c$), 7.10 (dd, [3]J_{HH} = 5.7 Hz, [4]J_{HH} = 0.8 Hz, 2H, H$_i$), 6.98 (td, [3]J_{HH} = 7.6 Hz, [4]J_{HH} = 1.3 Hz, 2H, H$_b$), 6.91 (d, [2]J_{HH} = 2.0 Hz, 2H, H$_d$), 6.75 (td, [3]J_{HH} = 7.4 Hz, [4]J_{HH} = 1.2 Hz, 2H, H$_e$), 6.45 (dd, [3]J_{HH} = 7.4 Hz, [4]J_{HH} = 1.1 Hz, 2H, H$_f$), 3.03 (s, 6H, H$_g$) 2.60 (s, 6H, H$_j$) ppm. ^{13}C NMR (100 MHz, CDCl3): δ 170.6 (NCN), 156.1, 151.0, 150.2, 146.4, 137.4, 133.9, 128.2, 126.2, 125.7, 122.3, 122.1, 114.9, 111.6 (ArC), 35.3 (NCH_3), 21.3 (CH_3) ppm. ^{31}P NMR (81 MHz, CDCl3): δ −144.3 (sept, [1]J_{PF} = 713 Hz, PF_6) ppm. HRMS (ESI-TOF) m/z (%): calcd. 691.2163; found 691.2166 (100) $[(M − PF_6)^+]$.

cis-3. Pure **cis-3** (30 mg, 0.04 mmol, 6% yield based on 4,4′-dimethyl-2,2′-bipyridine) was obtained as yellow crystals. ^{1}H NMR (400 MHz, CDCl3): δ 8.13 (s, 1H, ArH), 8.08 (s, 1H, ArH), 8.04 (d, [3]J_{HH} = 5.6 Hz, 1H, ArH), 7.73 (d, [3]J_{HH} = 6.0 Hz, 1H, ArH), 7.48 (d, [3]J_{HH} = 2.0 Hz, 1H, ArH), 7.40 (d, [3]J_{HH} = 2.0 Hz, 1H, ArH), 7.21 (dd, [3]J_{HH} = 6.0 Hz, [4]J_{HH} = 0.8 Hz, 1H, ArH), 7.17 (td, [3]J_{HH} = 7.6 Hz, [4]J_{HH} = 0.8 Hz, 2H, ArH), 7.09 (dd, [3]J_{HH} = 5.6 Hz, [4]J_{HH} = 1.0 Hz, 1H, ArH), 7.04−6.97 (m, 2H, ArH), 6.95 (d, [2]J_{HH} = 2.0 Hz, 1H, ArH), 6.84 (d, [3]J_{HH} = 2.4 Hz, 1H, ArH), 6.77 (td, [3]J_{HH} = 7.6 Hz, [4]J_{HH} = 1.0 Hz, 1H, ArH), 6.69 (td, [3]J_{HH} = 7.6 Hz, [4]J_{HH} = 1.0 Hz, 1H, ArH), 6.52 (dd, [3]J_{HH} = 7.6 Hz, [4]J_{HH} = 1.2 Hz, 1H, ArH), 6.10 (dd, [3]J_{HH} = 7.2 Hz, [4]J_{HH} = 0.8 Hz, 1H, ArH), 3.12 (s, 3H, NCH_3), 3.09 (s, 3H, NCH_3), 2.59 (s, 3H, CH_3), 2.49 (s, 3H, CH_3) ppm. ^{13}C NMR (100 MHz, CDCl3): δ 156.6, 156.4, 154.6, 152.1, 150.9, 150.2, 138.0, 132.0, 129.5, 128.3 126.0, 125.7, 124.4, 124.6, 122.9, 122.9, 122.8, 122.7, 115.0, 114.9, 111.4, 111.1 (ArC), 36.2 (NCH_3), 35.8 (NCH_3), 21.6 (CH_3), 21.5 (CH_3)

ppm. ^{31}P NMR (81 MHz, CDCl$_3$): δ −144.4 (sept, $^1J_{PF}$ = 713 Hz, PF$_6$) ppm. HRMS (ESI-TOF) m/z (%): calcd. 691.2163; found 691.2153 (100) [(M − PF$_6$)$^+$].
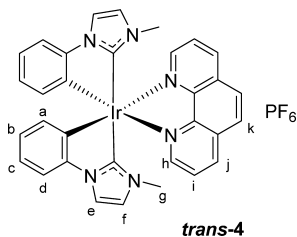
***trans*-4**

***trans*-4**. A solution of 216 mg (1.2 mmol, 3 equiv) of 1,10-phenanthroline and 356 mg (0.4 mmol, 1 equiv) of [**Ir(Ph-Im)$_2$(μ-Cl)**]$_2$ in 20 mL of CH$_2$Cl$_2$ was stirred overnight under nitrogen at room temperature. Then the dark solution was concentrated, and the crude product was prepurified on a short plug of silica gel using 2% of acetone in CH$_2$Cl$_2$ as solvent. After removing impurities, KPF$_6$ in acetone was used as the eluent to elute the product as the corresponding PF$_6$ salt. The solvent was removed in vacuo, and the solid was redissolved in CH$_2$Cl$_2$ and filtered through cotton to remove excess of KPF$_6$. The product was purified on silica gel using 2% of acetone in CH$_2$Cl$_2$ as solvent. 107 mg (0.13 mmol, 16% based on [**Ir(Ph-Im)$_2$(μ-Cl)**]$_2$) of the pure product were obtained as orange solid. ^{1}H NMR (400 MHz, CDCl$_3$): δ 8.61 (dd, $^3J_{HH}$ = 8.2 Hz, $^4J_{HH}$ = 1.4 Hz, 2H, H$_h$), 8.44 (dd, $^3J_{HH}$ = 5.1 Hz, $^4J_{HH}$ = 1.4 Hz, 2H, A H$_j$), 8.17 (s, 2H, H$_k$), 7.74 (dd, $^3J_{HH}$ = 8.2 Hz, $^3J_{HH}$ = 5.1 Hz, 2H, H$_i$), 7.47 (d, $^3J_{HH}$ = 2.1 Hz, 2H, H$_a$), 7.21 (dd, $^3J_{HH}$ = 7.9 Hz, $^4J_{HH}$ = 1.1 Hz, 2H, H$_c$), 7.03 (td, $^3J_{HH}$ = 7.6 Hz, $^4J_{HH}$ = 1.4 Hz, 2H, H$_b$), 6.87 (d, $^3J_{HH}$ = 2.0 Hz, 2H, H$_d$), 6.82 (td, $^3J_{HH}$ = 7.4 Hz, $^4J_{HH}$ = 1.3 Hz, 2H, H$_e$), 6.57−6.55 (m, 2H, H$_f$), 2.75 (s, 6H, H$_g$) ppm. ^{13}C NMR (100 MHz, CDCl$_3$): δ 170.0 (NCN), 151.7, 147.7, 146.5, 137.6, 137.5, 132.5, 131.3, 128.4, 126.4, 126.1, 122.7, 122.3, 115.0, 111.8 (ArC), 35.2 (NCH$_3$) ppm. ^{31}P NMR (81 MHz, CDCl$_3$): δ −144.4 (sept, $^1J_{PF}$ = 713 Hz, PF$_6$) ppm. HRMS (ESI-TOF) m/z (%): calcd. 687.1850; found 687.1841 (100) [(M − PF$_6$)$^+$].
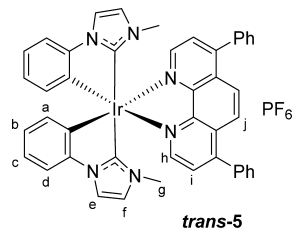
***trans*-5**

***trans*-5**. A solution of 199 mg (0.6 mmol, 1.5 equiv) of 4,7-diphenyl-1,10-phenanthroline, and 356 mg (0.4 mmol, 1 equiv) of [**Ir(Ph-Im)$_2$(μ-Cl)**]$_2$ in 20 mL of CH$_2$Cl$_2$ was stirred overnight under nitrogen at room temperature. Then the dark solution was concentrated and the crude product was prepurified on a short plug of silica gel using 2% of acetone in CH$_2$Cl$_2$ as solvent. After removing impurities, KPF$_6$ in acetone was used as the eluent to elute the product as the corresponding PF$_6$ salt. The solvent was removed in vacuo and the solid was redissolved in CH$_2$Cl$_2$ and filtered through cotton to remove excess of KPF$_6$. The product was purified on silica gel using CH$_2$Cl$_2$ and then 2% of acetone in CH$_2$Cl$_2$ as solvent. 152 mg (0.15 mmol, 26% based on 4,7-diphenyl-1,10-phenanthroline) of the pure product were obtained as red solid. ^{1}H NMR (400 MHz, CDCl$_3$): δ 8.39 (d, $^3J_{HH}$ = 5.3 Hz, 2H, H$_h$), 8.04 (s, 2H, A H$_j$), 7.52−7.45 (m, 12H, H$_i$, Ph), 7.37 (d, $^3J_{HH}$ = 2.1 Hz, 2H, H$_a$), 7.11 (dd, $^3J_{HH}$ = 7.8 Hz, $^4J_{HH}$ = 1.1 Hz, 2H, H$_c$), 6.92 (td, $^3J_{HH}$ = 7.6 Hz, $^4J_{HH}$ = 1.3 Hz, 2H, H$_b$), 6.87 (d, $^3J_{HH}$ = 2.0 Hz, 2H, H$_d$), 6.72 (td, $^3J_{HH}$ = 7.4 Hz, $^4J_{HH}$ = 1.2 Hz, 2H, H$_e$), 6.49 (dd, $^3J_{HH}$ = 7.4 Hz, $^4J_{HH}$ = 1.2 Hz, 2H, H$_f$), 2.79 (s, 6H, H$_g$) ppm. ^{13}C NMR (100 MHz, CDCl$_3$): δ 169.8 (NCN), 151.3, 150.0, 148.3, 146.6, 137.6, 135.5, 133.0, 129.9, 129.8, 129.3, 129.2, 126.3, 126.2, 126.1, 122.7, 122.6, 115.0, 111.8 (ArC), 35.4 (NCH$_3$) ppm. ^{31}P NMR (81 MHz, CDCl$_3$): δ −144.6 (sept, $^1J_{PF}$ = 713 Hz, PF$_6$) ppm. HRMS (ESI-TOF) m/z (%): calcd. 839.2477; found 839.2478 (100) [(M − PF$_6$)$^+$].

■ RESULTS AND DISCUSSION

Synthesis and X-ray Crystal Structures. The carbene-type ligand has been obtained from 3-methyl-1-phenyl-1H-imidazol-3-ium iodide, synthesized by alkylation of commercially available 1-phenylimidazole with CH$_3$I, as described previously (Scheme 1).[17,55,56] The product was precipitated from toluene as white solid in 92% yield. The standard preparation method of Ir complexes based on the [Ir(ppy)$_2$(μ-Cl)]$_2$ dimer (where Hppy = 2-phenylpyridine) affords very poor reaction yields with carbene ligands; therefore, we used the recently reported [Ir(COD)(μ-Cl)]$_2$ (COD = 1,5-cyclooctadiene) as key intermediate.[18] Instead of deprotonation of the imidazolium salt with a strong base to form the free carbene, we used Ag$_2$O as a transmetalating agent. This procedure allows the in situ generation of the corresponding silver carbene complex, which then transfers the ligand to [Ir(COD)(μ-Cl)]$_2$, affording the desired dimer [**Ir(Ph-Im)$_2$(μ-Cl)**]$_2$ (Ph-Im = 3-methyl-1-phenyl-imidazol) as depicted in

Scheme 1. Synthesis of Cationic Iridium(III) Complexes *cis*-3 and *trans*-3
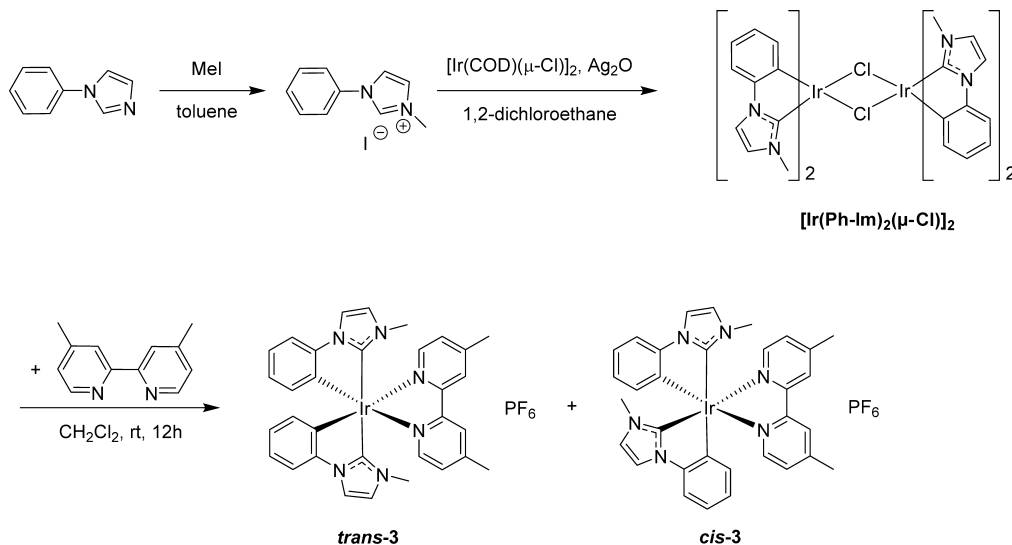
Scheme 1. The crude product was isolated as a brown solid, which was utilized without further purification. Recently, this compound was synthesized in situ and used without isolation.[17] The ^{1}H NMR spectrum of the Ir dimer was rather complex and difficult to interpret, indicating the presence of geometrical isomers.

4,4′-Dimethylbipyridine was tested as the first ancillary ligand; 111 mg (0.4 mmol) were left with the aforementioned dimer (356 mg; 0.6 mmol) at room temperature in CH_2Cl_2 overnight (Scheme 1). A mixture of the two isomers was observed and separated by column chromatography on silica gel as PF_6 salts. The **trans-3** was obtained as the major product (20% yield), whereas **cis-3** was isolated in only 6% yield. To obtain only the thermodynamically more stable product, the reaction was repeated at higher temperature (80 °C in 1,2-dichloroethane instead of CH_2Cl_2) for 12 h. However, a mixture of isomers with roughly the same composition as before was observed. De Cola et al. also observed a mixture of cis and trans isomers when N,N-cis-[Ir(C^N)$_2$(Cl)]$_2$ (C^N = phenyl-triazole) dimer was reacted with bipyridine derivatives, while the pure N,N-trans dimer resulted in pure N,N-trans product. These findings indicate that the synthesis of the iridium dimer, rather than its cleavage, is crucial for the stereochemistry of the final product, and De Cola and co-workers reported a complete control of stereochemistry by changing the reaction temperature upon dimer preparation.[23] Anyway, since we were able to successfully isolate both isomers in pure form, no further attempts were made to find reaction conditions leading to the individual thermodynamic product.

The other complexes of the series were prepared by replacing 4,4′-dimethylbipyridine with other substituted bipyridine or phenanthroline ligands (Scheme 2). The reaction time was kept

Scheme 2. Structures of Cationic Iridium(III) Complexes *trans*-1−5

R = OMe (**trans-1**), ^{t}Bu (**trans-2**), Me (**trans-3**)   R = H (**trans-4**), Ph (**trans-5**)

at 12 h, and the stoichiometry was tuned from excess of dimer to excess of ligand. However, the change in stoichiometry did not significantly affect the final result, and the reaction yields were not improved. In all cases the trans isomer was obtained as the major product and isolated in pure form. The isolation of the pure cis complexes of **1**, **2**, **4**, and **5** was difficult, and all attempts to grow single crystals from the ∼95% pure cis products after chromatography failed.

Single crystals suitable for X-ray diffraction analysis were grown by slow diffusion of heptane into a dichloromethane solution of the complexes **cis-3** and **trans-4**. The **cis-3** complex crystallizes with half a molecule of water, likely from acetone used for the column chromatography that had not been dried prior to use, while **trans-4** crystallizes with a molecule of dichlormethane. In both complexes the iridium atom is engaged in a slightly distorted octahedral coordination. The perspective views of both complexes are shown in Figure 1, and selected bond distances and angles are listed in Table 1, while the crystallographic data are reported in Supporting Information, Table S1. In contrast to the archetype compounds [Ir-(ppy)$_2$(L^L)]PF$_6$ (ppy = 2-phenylpyridine or 2-(2,4-difluorophenyl)pyridine and L^L = bis-carbene or pyridine-carbene), where the pyridine groups of the cyclometallating ppy ligands are always in trans orientation to each other,[31] in this series we observed cis and trans isomers. In both cases the C(1)−Ir(1)−C(19) angle deviates from linearity with 169.74(7)° for **cis-3** and 167.4(3)° for **trans-4**. These values are similar to the N−Ir−N angles in [Ir(ppy)$_2$(L^L)]PF$_6$ compounds (168.11° to 171.31°).[31] In comparison to these complexes, the Ir−C$_{aryl}$ bond length in **trans-4** (Ir−C(11), 2.067(6) Å) and **cis-3** (Ir−C(19), 2.0783(19) Å)—in trans orientation to a pyridine and a carbene group, respectively—are similar within the experimental error. The stronger trans-influence of the carbene over the pyridine[57] becomes more pronounced for the Ir−C$_{carbene}$ bond length. When the carbene carbon atom is in trans orientation to a pyridine (**cis-3**), a very short Ir−C$_{carbene}$ length is observed (Ir−C(11) 1.9945(18) Å), while in **trans-4** (carbene centers in trans position) a significantly longer Ir−C$_{carbene}$ bond length is observed (Ir−C(1) 2.051(7) Å and Ir−C(19) 2.060(7) Å). The bond lengths of the mutually trans Ir−C$_{carbene}$ bonds (Ir−C(1), Ir−C(19) average 2.056(7) Å) are longer than those reported for the neutral homoleptic iridium complex *mer*-[Ir(pmb)$_3$] (pmb = 1-phenyl-3-methylbenzimidazolin-2-ylidene) (average mutually trans Ir−C$_{carbene}$ 2.026(4) Å) and for the neutral bis-
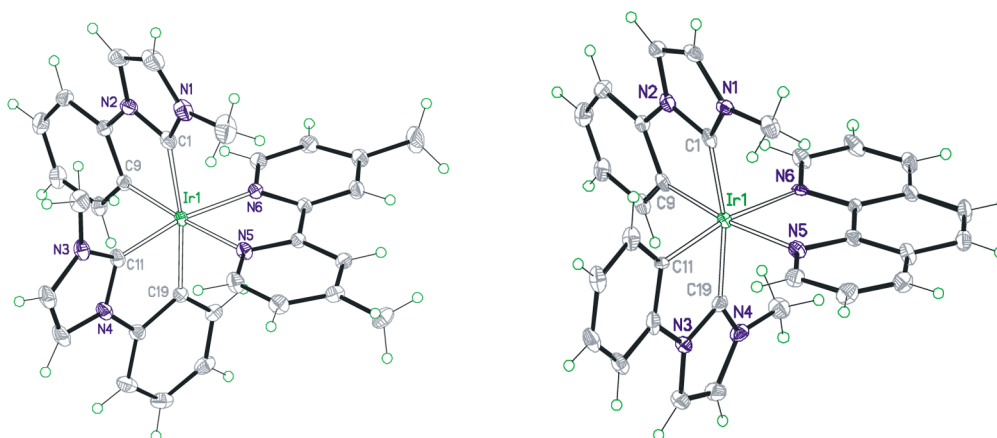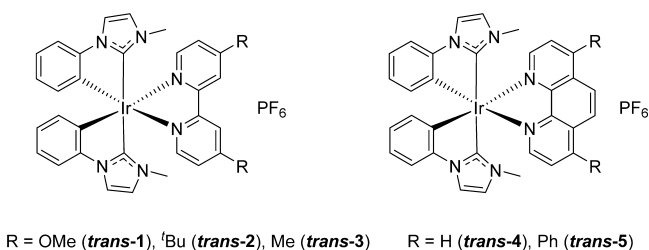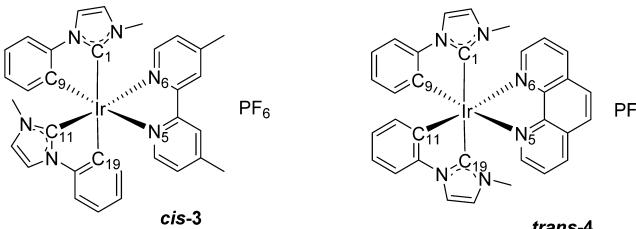

Figure 1. Perspective view of **cis-3** (left) and **trans-4** (right); PF$_6$ anions and cocrystallized solvent molecules are omitted for clarity.

Table 1. Selected Bond Distances (Å) and Angles (deg) for cis-3 and trans-4

cis-3

trans-4

| distances	*cis*-3	*trans*-4
Ir−N$_5$	2.1176(16)	2.134(6)
Ir−N$_6$	2.1038(16)	2.125(5)
Ir−C$_1$	2.063(2)	2.051(7)
Ir−C$_9$	2.0513(19)	2.041(7)
Ir−C$_{11}$	1.9945(18)	2.067(6)
Ir−C$_{19}$	2.0783(19)	2.060(7)
angles		
C(11)−Ir(1)−C(9)	88.13(7)	95.0(2)
C(11)−Ir(1)−C(1)	96.66(8)	92.3(2)
C(9)−Ir(1)−C(1)	78.52(8)	78.4(3)
C(11)−Ir(1)−C(19)	79.22(8)	78.5(3)
C(9)−Ir(1)−C(19)	91.90(7)	93.7(3)
C(1)−Ir(1)−C(19)	169.74(7)	167.4(3)
C(11)−Ir(1)−N(6)	169.60(7)	169.0(2)
C(9)−Ir(1)−N(6)	98.94(7)	94.5(2)
C(1)−Ir(1)−N(6)	92.24(7)	95.0(2)
C(19)−Ir(1)−N(6)	92.86(7)	95.4(2)
C(11)−Ir(1)−N(5)	95.90(7)	92.5(2)
C(9)−Ir(1)−N(5)	175.86(7)	171.9(2)
C(1)−Ir(1)−N(5)	99.99(7)	98.1(2)
C(19)−Ir(1)−N(5)	89.81(7)	90.9(2)
N(6)−Ir(1)−N(5)	77.20(6)	78.4(2)

(heteroleptic) iridium complex *trans*-[Ir(CNpmi)$_2$(pic)] (CNpmi = 1-(4-cyanophenyl)-3-methylimidazolin-2-ylidene; pic = picolate) (average mutually trans Ir−C$_{carbene}$ 2.032(5) Å). These findings may be related to the charged nature of complex *trans*-4. Finally, it must be noted that the overall influence of the different ancillary ligands (bipyridine/phenanthroline) on the solid-state structure is negligible.

Electrochemistry. The redox potentials of the complexes were obtained by CV versus ferrocenium/ferrocene (Table 2 and Figure 2). The oxidation potentials of *trans*-1−5 are in the range of 0.69−0.74 V; notably, that of *cis*-3 is 100 mV higher (0.82 V) compared to *trans*-3 (0.72 V). The electrochemical gap decreases from *cis*-3 (2.86 eV) to *trans*-1−3 (2.68−2.64 eV) and then to *trans*-4 (2.60 eV) and *trans*-5 (2.54 eV), as expected from the observed red shift of the emission band

Table 2. Electrochemical Properties of Complexes 1−5 from CV Data in Acetonitrile/TBAPF$_6$ 0.1 M Versus Fc$^+$/Fc

|	E_{ox}[a] (V)	E_{red}[a] (V)	$E_{ox} - E_{red}$ (V)
trans-1	0.69	−1.95	2.64
trans-2	0.72	−1.96	2.68
trans-3	0.72	−1.95	2.67
cis-3	0.82	−2.04	2.86
trans-4	0.73	−1.87	2.60
trans-5	0.74	−1.80	2.54

[a]$E = 1/2(E_{pa} + E_{pc})$.
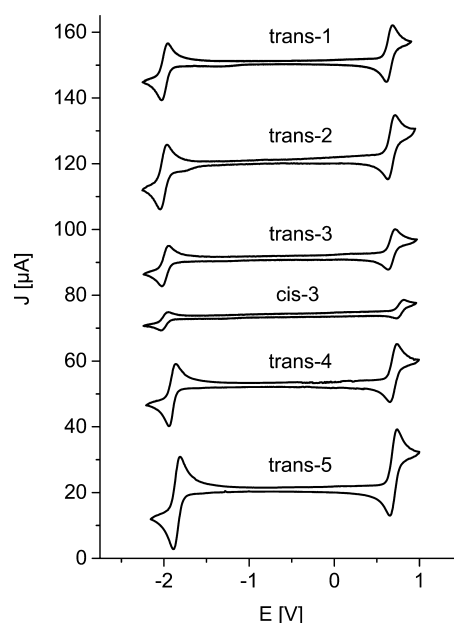
Figure 2. Cyclic voltammograms of *trans*-1−5 and *cis*-3 recorded in acetonitrile/TBAPF$_6$ 0.1 M vs Fc$^+$/Fc (different intensities are due to different concentrations of the complexes used).

maxima (Figure 5). A 30 mV cathodic shift is observed for the oxidation potential of the stronger donor-substituted complex *trans*-1 (Scheme 2, R = OMe) compared to complex *trans*-3 (R = Me). A similar shift is observed in literature for an iridium(III) complex with two 2-(2-pyridyl)benzo[*b*]thiophene cyclometalating ligands and identically substituted bipyridine ancillary ligands.[58] On the other hand, the described cathodic shift of 20 mV for the reduction potential was not found in our study. The minor differences in donor strength of the substituents on the 2,2′-bipyridine ligands seem to be overcompensated by the strongly donating carbene groups, resulting in an ~150 mV cathodic shift of complexes *trans*-1 and *trans*-3 when compared to its corresponding 2-(2-pyridyl)benzo[*b*]thiophene iridium complexes.[58]

Both, oxidation and reduction processes show excellent reversibility throughout the entire series, as rarely observed for analogous luminescent iridium complexes. High stability can therefore be expected in electroluminescent devices. This is surprising because the complex [Ir(pmi)$_2$(bipy)]Cl (pmi = 1-phenyl-3-methylimidazolin-2-ylidene; bipy = 2,2′-bipyridine), which is very similar to *trans*-3, exhibits an irreversible oxidation process in dimethylformamide at 0.75 V versus Fc$^+$/Fc.[17] On the other hand, the reversible reduction process of the above-mentioned complex at −1.89 V versus Fc$^+$/Fc is in line with our findings for *trans*-3 (−1.95 V vs Fc$^+$/Fc), taking into account the different solvents used.[17] Finally, only minor differences in redox potentials within the subgroups of bipyridine and phenanthroline ancillary ligands are found. In Supporting Information, Figure S1 a graphical representation of highest occupied molecular orbital (HOMO) and lowest unoccupied molecular orbital (LUMO) levels of complexes *trans*-1−5 and *cis*-3 based on CV measurements can be found.

Theoretical Calculations on the Electronic Ground State. The molecular structures and electronic properties of complexes *cis*-3 and *trans*-3−4 were investigated by DFT calculations and compared with those of X-ray crystallographic structures and electrochemical data. The PBE0 hybrid func-
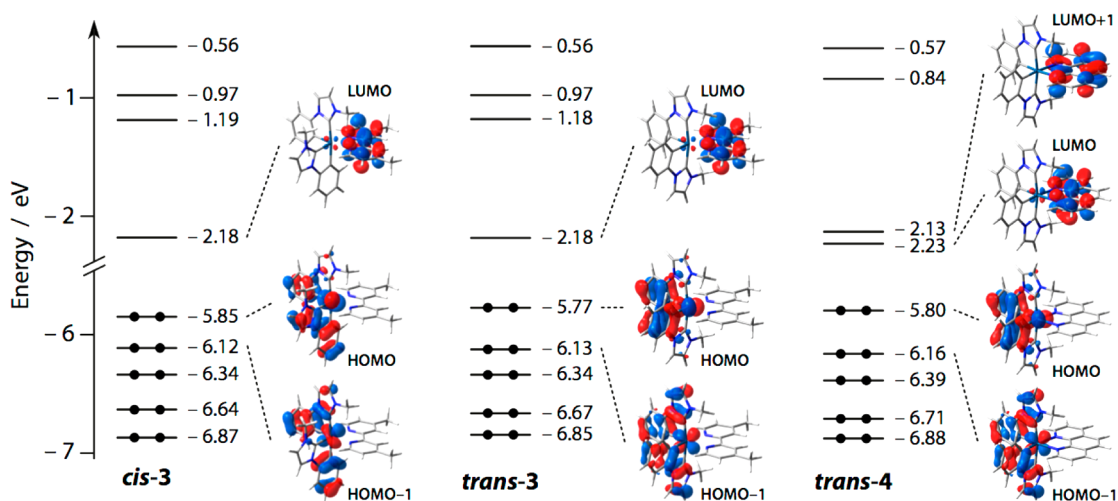
Figure 3. Energy diagram showing the energy values of frontier Kohn−Sham molecular orbitals of *cis*-3 and *trans*-3−4 in acetonitrile; for some relevant orbitals, the corresponding isosurface is also displayed for the sake of clarity (isovalue = 0.04 $e^{1/2}$ $bohr^{-3/2}$).

tional[41,42] was used together with the 6-31G(d,p) basis set for C, H, and N atoms,[43] and the LANL2DZ pseudopotential was used on the Ir(III) metal center[44] (see the Experimental Section). The ground-state (S_0) geometry was fully optimized without symmetry constraints in the presence of the solvent using the PCM (in acetonitrile).[45−47] The quality of the calculated structures was evaluated by comparison with the X-ray structures of *cis*-3 and *trans*-4. In Supporting Information, Figure S2 the structural overlaps between the available crystallographic geometries and the theoretically computed ones are reported. All the calculated structures do not noticeably differ from experimental data as the minimized root-mean-square deviation of all the atomic positions (except hydrogen atoms) is 0.163 and 0.221 Å for *cis*-3 and *trans*-4, respectively.[59]

The frontier molecular orbitals of *cis*-3 and *trans*-3−4 are depicted in Figure 3. As usually found for cyclometalated cationic iridium(III) complexes, the HOMO is mainly localized on the metal center and on the phenyl moiety of the cyclometalating ligands, while the LUMO is centered on the diimine ancillary ligand. If compared to the archetypal complex [Ir(ppy)$_2$(bpy)]$^+$, the presence of the phenyl−carbene cyclometalating ligand induces a destabilization of the HOMO of ∼0.18 eV for *trans*-3 and 0.10 eV for *cis*-3. These values are in line with the oxidation potentials reported in Table 2 (for graphically represented HOMO and LUMO levels see also Supporting Information, Figure S1), if compared to the value of [Ir(ppy)$_2$(bpy)]$^+$ (+0.84 V).[7] In the cis and trans isomers [Ir(C^N)$_2$(N^N)]$_2$ (C^N = phenyl-triazole, N^N = 4,4′-dimethyl-2,2′-bipyridine) reported by De Cola and co-workers the strongly electron-accepting triazole group stabilizes the frontier orbitals, while our donating carbene groups destabilizes them.[23] This results in a higher-lying HOMO level by 2.11 eV for *cis*-3 and 2.07 eV for *trans*-3 compared to the triazole complexes and is even more pronounced for the LUMO levels (ΔE = 2.57 eV for cis and 2.46 eV for trans complexes) strongly located on the diimine ancillary ligand in both classes of complexes. While in the triazole series the LUMO is more stabilized in the case of the cis complex than in the trans analogue (resulting in a decreased gap and therefore a red shift in emission),[23] in the present study CV measurements indicate,

that the LUMO is more destabilized in *cis*-3 than it is in *trans*-3 (resulting in an increased gap and blue shift in emission).

It should be emphasized that the two isomers *cis*-3 and *trans*-3 exhibit virtually identical MO diagrams, with only a slightly smaller HOMO energy of the former (0.08 eV). This theoretical finding is again experimentally validated since the oxidation potential of *cis*-3 is 0.10 V higher than that of *trans*-3 (Table 2). On the other hand, comparison of *trans*-3 and *trans*-4 shows that the energy associated with the LUMO+1 of the latter is very close to that of the LUMO. This is a common feature of bipyridine- versus phenanthroline-based cyclometalated iridium(III) complexes, sometimes leading to peculiar photophysical properties.[60] Consequently, the HOMO−LUMO energy gap is wider for *cis*-3 (3.67 eV), while both *trans*-3 and *trans*-4 complexes display smaller and comparable values (3.59 and 3.57 eV, respectively). This trend is in excellent agreement with the electrochemical gaps obtained experimentally by cyclic voltammetry (2.86, 2.67, and 2.60 eV, respectively). According to calculations, a blue shift is therefore expected in both the absorption and emission spectra of *cis*-3 compared to *trans*-3, while the photophysical properties of the investigated trans complexes are expected to be similar.

Photophysical Properties in Organic Solvents. All of the investigated complexes are stable in both CH$_3$CN and CH$_2$Cl$_2$ solutions for months and do not show any degradation under standard experimental conditions, including irradiation. The room-temperature UV−vis absorption spectra of complexes *trans*-1−5 and *cis*-3 in CH$_3$CN are reported in Figure 4.

The spectral window between 200 and 300 nm is characterized by strong absorption bands with molar absorptivities (ε) higher than 2×10^4 M^{-1} cm^{-1}. These bands originate from spin-allowed $^1(\pi−\pi^*)$ ligand-centered (LC) transitions involving both the cyclometalating and the ancillary ligands. The most intense absorption band in this spectral window is observed for *trans*-5, due to the presence of the strong $\pi−\pi^*$ transitions centered on the bathophenanthroline (4,7-diphenyl-1,10-phenanthroline) ancillary ligand (Scheme 2). At longer wavelengths (λ > 300 nm; Figure 4, magnified region), several weaker and broader bands are present in all cases and are attributed to charge-transfer transitions with mixed metal-to-ligand and ligand-to-ligand
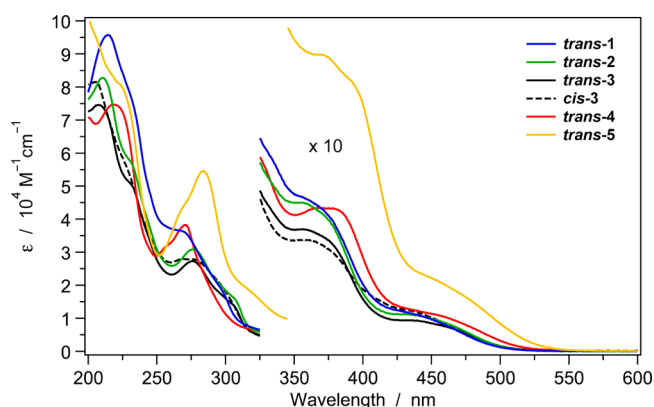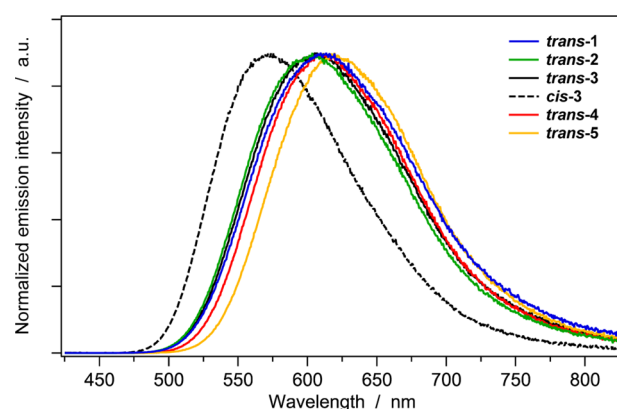
Figure 4. Absorption spectra of *trans*-**1**−**5** and *cis*-**3** in CH$_3$CN at 298 K. The lower-energy bands are magnified by a factor of 10 for the sake of clarity.

Figure 5. Normalized emission spectra of *trans*-**1**−**5** and *cis*-**3** in CH$_3$CN at 298 K (λ_{exc} = 375 nm).

charge transfer (MLCT and LL′CT) character with both singlet and triplet spin multiplicity, due to the high intersystem-crossing efficiency promoted by the Ir(III) metal ion.[7,8] To corroborate the attribution of the experimental absorption bands, the first 100 singlet vertical excitations calculated by TD-DFT are reported for *trans*-**3**−**4** and *cis*-**3**; they compare well with their corresponding experimental absorption spectra (Supporting Information, Figures S3−S5). To elucidate the nature of the lowest absorption transitions and get a clear picture of the energy distribution of the potentially emitting states of these complexes, also the first 12 triplet vertical excitations were computed. The lowest ones are reported in Table 3 and in Table S2 (Supporting Information) using the natural transition orbital (NTO) representation for the electronic transition density matrix.[61] TD-DFT calculations confirm the indications provided by the molecular orbitals of *trans*-**3**−**4** and *cis*-**3** (Figure 3), since the first triplet excited state results mainly from a HOMO → LUMO excitation, therefore exhibiting a predominant MLCT character with an LL′CT contribution.

The room-temperature emission spectra of complexes *trans*-**1**−**5** and *cis*-**3** in CH$_3$CN solution are collected in Figure 5. All the complexes display a broad emission band, a further indication that the emissive excited states have a pronounced MLCT/LL′CT character.[7] The charge-transfer nature of the excited states is further suggested by the blue shift of the

emission maxima observed upon lowering the polarity of the solvent (see Table 3 and the emission spectra in CH$_2$Cl$_2$ in Figure S6, Supporting Information). All of the trans complexes (*trans*-**1**−**5**) show emission maxima at ∼612 nm (±8 nm, depending on the N^N ligand); hence, the neutral ancillary ligand has a limited effect on the emission energy. Minor differences are found for the phenanthroline-based systems (*trans*-**4**−**5**) showing lower-energy emission bands compared to bipyridine-type analogues (*trans*-**1**−**3**), a finding commonly observed in other series of cationic iridium(III) complexes.[60,62−64] On the other hand, the emission of *cis*-**3** is substantially higher in energy with respect to the trans complexes. In particular, if *cis*-**3** is compared to its geometrical isomer *trans*-**3**, a blue shift of more than 30 nm is observed, which corresponds to an energy difference of 0.12 eV.

These experimental findings are in excellent agreement with spin-unrestricted DFT calculations carried out by fully optimizing the lowest triplet state (T$_1$). After a complete geometry relaxation, T$_1$ preserves its MLCT/LL′CT character as revealed by the spin-density distribution depicted in Figure 6 for *cis*-**3** and *trans*-**3**. Moreover, the calculated emission energy (see Experimental section) is estimated to be 1.95 versus 1.86 eV for *cis*-**3** and *trans*-**3**, respectively. These theoretical results slightly underestimate the experimental spectral values of both complexes by ∼0.20 eV. However, they fit well the observed difference of 0.10 eV in oxidation potential and 0.12 eV in emission energy between *cis*-**3** and *trans*-**3**.

Table 3. Lowest Triplet Vertical Excitations (below 3.00 eV) Calculated at the PBE0/6-31G(d,p)&LANL2DZ Level of Theory for *cis*-3 and *trans*-3−4 in Acetonitrile (using PCM)

complex	state	transition energy [eV (nm)]	description[a]	nature
cis-**3**	T$_1$	2.72 (456)	π_{Ph} + d$_\pi$ (Ir) → π^*_{bpy}	^{3}MLCT/^{3}LL′CT
	T$_2$	2.97 (417)	π_{Ph} + d$_\pi$ (Ir) → π^*_{bpy}	^{3}MLCT/^{3}LL′CT
	T$_3$	2.99 (415)	π_{bpy} + d$_\pi$ (Ir) → π^*_{bpy}	^{3}MLCT/^{3}LC
trans-**3**	T$_1$	2.68 (463)	π_{Ph} + d$_\pi$ (Ir) → π^*_{bpy}	^{3}MLCT/^{3}LL′CT
	T$_2$	2.94 (421)	π_{bpy} + d$_\pi$ (Ir) → π^*_{bpy}	^{3}MLCT/^{3}LC
	T$_3$	2.97 (417)	π_{crb} + d$_\pi$ (Ir) → π^*_{bpy}	^{3}MLCT/^{3}LL′CT
trans-**4**	T$_1$	2.59 (479)	π_{phen} + d$_\pi$ (Ir) → π^*_{phen}	^{3}MLCT/^{3}LC
	T$_2$	2.72 (456)	π_{Ph} + π_{phen} + d$_\pi$ (Ir) → π^*_{phen}	^{3}MLCT/^{3}LC
	T$_3$	2.87 (432)	$\pi_{C^\wedge C}$ + d$_\pi$ (Ir) → π^*_{phen}	^{3}MLCT/^{3}LL′CT
	T$_4$	2.94 (421)	$\pi_{C^\wedge C}$ + d$_\pi$ (Ir) → π^*_{phen}	^{3}MLCT/^{3}LL′CT

[a]Ph = phenyl moiety of the cyclometalating ligands; bpy = 2,2′-bipyridine; phen = 1,10-phenanthroline; crb = carbene moiety of the cyclometalating ligands; C^C = whole cyclometalating ligands. See Supporting Information, Table S2 for a better description of the transitions in terms of natural transition orbitals (NTOs).
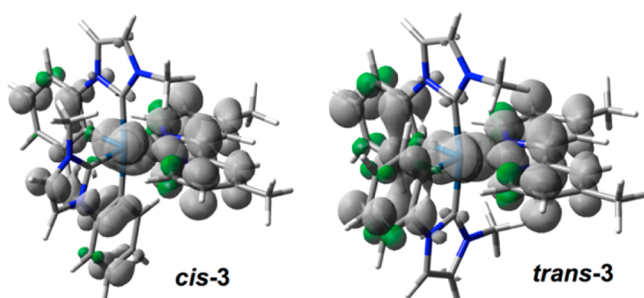
Figure 6. Spin-density distributions calculated for the fully relaxed lowest triplet state of *cis-3* and *trans-3* in acetonitrile (isovalue: 0.002 e bohr^{-3}).

Figure 7. Normalized emission spectra of *trans-1−5* and *cis-3* in CH$_3$CN at 77 K (λ_{exc} = 375 nm).

In room-temperature solutions, all *trans*-complexes display photoluminescence quantum yields (Φ_{PL}, Table 4) that are comparable to those of standard nonfluorinated cationic iridium(III) complexes with MLCT/LL′CT states.[7,64] It can be noticed that complexes with a phenanthroline-based ancillary ligand exhibit higher Φ_{PL} than those with a bipyridine-type ligand. This is a common feature in cyclometalated cationic iridium(III) complexes that have already been observed for phenyl−pyridine-[63,64] and phenyl−tetrazole-based[60] complexes.

It is worth noticing that *cis-3* displays a twofold increase of Φ_{PL} with respect to *trans-3* in CH$_2$Cl$_2$; an even higher increase (×4) is found in more polar and more coordinative acetonitrile (Table 4). Assuming a unitary intersystem crossing efficiency, the radiative and the overall nonradiative rate constants (k_r and k_{nr}, respectively) were calculated from Φ_{PL} and τ values,[7] and they are summarized in Table 4. Even though *cis-3* generally displays slightly lower k_r values compared to trans complexes, its superior Φ_{PL} can be primarily attributed to drastically slower nonradiative processes, as *trans-3* shows k_{nr} values over six times higher than those of *cis-3* in CH$_3$CN (Table 4).

At 77 K, the emission bands of all the complexes in CH$_3$CN exhibit slightly more structured profiles and undergo a considerable blue shift if compared to 298 K (Figure 7). This finding further corroborates the MLCT/LL′CT nature of the excited state. Interestingly, the rigidochromic effects causing the hypsochromic shift are more pronounced for the trans series: *trans-3* exhibits a blue shift of 56 nm (0.21 eV), whereas for *cis-3* this becomes only 29 nm (0.12 eV), so that the two compounds display almost superimposable emission bands at low temperature. This different photophysical behavior can be attributed to a different change in the dipole moment of the two isomers when passing from the ground state to the lowest triplet excited state. The *trans-3* complex exhibits a larger change in the dipole moment; accordingly, it shows the biggest
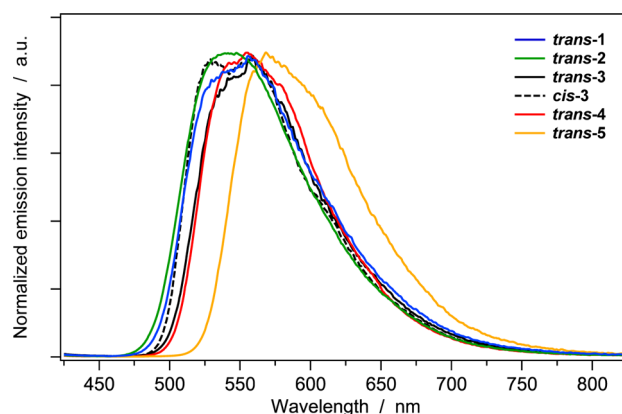
solvation effect in solution, and the highest hypsochromic shift at 77 K in rigid matrix (vide infra).

At low temperature, all complexes show bright luminescence of comparable intensity, when excited under the same experimental conditions. Therefore, the phosphorescence of all the trans complexes is strongly recovered at 77 K and becomes virtually equivalent to that of the *cis-3* isomer. The longer lifetime displayed by *cis-3* with respect to all the trans complexes can be rationalized by the slightly lower k_r value (Table 4), rather than assuming a peculiarly higher Φ_{PL} at 77 K. On the other hand, the recovery of *trans-3* phosphorescence at low temperature can be attributed to a sharp decrease of the nonradiative processes under these conditions. All these findings further indicate that significant nonradiative processes take place in trans complexes at room temperature, which are less relevant in *cis-3*. The different photophysical behavior of *cis-3* and *trans-3* at 298 K can be tentatively ascribed to (i) the presence of thermally activated nonradiative metal-centered states (^{3}MC) that are readily accessible in solution at 298 K for the trans complexes but become inaccessible at 77 K or in rigid polymeric matrix;[7,64] (ii) different vibronic coupling between the excited and the ground states that depends on the different stereochemistry; (iii) distinct solvation effects that lead to differently relaxed emitting states; (iv) a synergic combination of some of the above-mentioned effects.

Photophysical Properties in the Solid State. Photophysical studies were also carried out in the solid state, that is, in a diluted PMMA matrix (1% by weight) and as neat films (Table 5 and Supporting Information, Figures S6 and S7). In PMMA all of the complexes display a similar photophysical behavior with $\Phi_{PL} \approx 70−80\%$, comparable emission lifetimes ($\tau \approx 1.3\ \mu$s), and a remarkable rigidochromic shift (Supporting

Table 4. Photophysical Data of Complexes *trans-1−5* and *cis-3* in Solution at 298 K and in Rigid Matrix at 77 K

	CH$_3$CN oxygen-free solution, 298 K					CH$_2$Cl$_2$ oxygen-free solution, 298 K					CH$_3$CN rigid matrix, 77 K	
	λ_{em} (nm)	Φ_{PL} (%)	τ (ns)	k_r (1×10^5 s^{-1})	k_{nr} (1×10^6 s^{-1})	λ_{em} (nm)	Φ_{PL} (%)	τ (ns)	k_r (1×10^5 s^{-1})	k_{nr} (1×10^6 s^{-1})	λ_{em} (nm)	τ (μs)
trans-1	611	4.2	145	2.93	6.60	600	10.1	294	3.43	3.06	556	5.3
trans-2	604	12.0	362	3.33	2.43	583	29.3	708	4.13	1.00	542	5.0
trans-3	606	8.5	278	3.06	3.29	590	21.5	579	3.71	1.36	540^{sh}, 559	4.6
cis-3	573	31.1	1291	2.41	0.53	560	46.4	1777	2.61	0.30	529, 558	8.7
trans-4	612	14.5	509	2.85	1.68	593	32.2	890	3.62	0.76	555	5.4
trans-5	620	20.4	633	3.23	1.26	600	43.1	1056	4.08	0.54	569	5.7

Table 5. Photophysical Data of Complexes *trans*-1−5 and *cis*-3 in PMMA 1% w/w and in Neat Film at 298 K

	PMMA 1% w/w at 298 K					neat film at 298 K				
	λ_{em} (nm)	Φ_{PL} (%)	τ (μs)	k_r (1×10^5 s^{-1})	k_{nr} (1×10^5 s^{-1})	λ_{em} (nm)	Φ_{PL} (%)	τ (ns)	k_r (1×10^5 s^{-1})	k_{nr} (1×10^6 s^{-1})
trans-1	542	66	1.0	6.7	3.4	575	17	310	5.3	2.7
trans-2	552	74	1.0	7.3	2.6	589	22	416	5.2	1.9
trans-3	548	71	1.1	6.8	2.8	581	16	334	4.7	2.5
cis-3	529	83	1.9	4.5	0.9	563	28	775	3.5	1.3
trans-4	552	77	1.3	5.9	1.8	593	19	447	4.2	2.2
trans-5	567	81	1.6	5.2	1.3	617	21	453	4.6	1.7

Information, Figure S7). This trend resembles what was observed at 77 K and is rather different compared to room-temperature solution. On the other hand, in neat films photoluminescence quantum yields and excited-state lifetimes are decreased but to a lesser extent compared to analogous Ir(III) complexes with carbene-based ancillary ligands, and emission lifetimes display monoexponential decays.[31]

Temperature Dependence of Triplet Lifetimes. To understand which of the effects mentioned above is mainly responsible for the faster nonradiative decay processes occurring in room-temperature solution for *trans*-3 versus *cis*-3, we investigated the trend of excited-state lifetimes of these two stereoisomers between 77 and 450 K in oxygen-free propylene glycol solutions. This solvent was selected because (a) it forms a transparent glass at low temperature; (b) it exhibits a high boiling point; and (c) it shows a gradual variation of viscosity with temperature. Figure 8 displays the
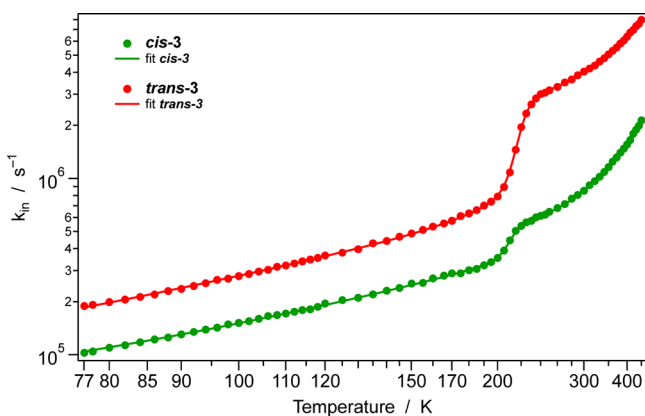
Figure 8. Temperature-dependent excited-state deactivation rates (k_{in} = 1/τ) of *cis*-3 and *trans*-3. The lines connecting the experimental points were fitted using eq 1 with two Arrhenius terms; the fitting parameters are reported in Table 6. Excited-state lifetimes were determined from the luminescence decays in oxygen-free propylene glycol solutions using the time-correlated single-photon counting technique (λ_{exc} = 407 nm).

evolution of the intrinsic deactivation rate constant (k_{in} = 1/τ, where τ is the excited-state lifetime of the emitting state) as a function of temperature. In general, the changes of k_{in} over a

wide temperature range can be modeled using the following equation:[41,64]

$$k_{in}(T) = k_0 + \frac{B}{1 + \exp\left[C\left(\frac{1}{T} - \frac{1}{T_g}\right)\right]} + \sum_i A_i \exp\left(-\frac{\Delta E_i}{k_B T}\right)$$

(eq 1)

where k_0 is a temperature-independent term, the second term (depending on B, C, and T_g values) takes into account the effect of the rigid-to-fluid transition of the sample, as extensively described in the literature.[64,65] On the other hand, the last term contains the summation of Arrhenius expressions, each of which contains a frequency factor (A_i) and the corresponding activation-energy barrier (ΔE_i).[64,65] Table 6 summarizes the values obtained for the parameters obtained from eq 1 after the nonlinear iterative fitting of experimental k_{in} data by introducing two Arrhenius terms. Both *cis*-3 and *trans*-3 exhibit a similar temperature-independent term ($k_0 \approx 5 \times 10^4$ s^{-1}), and it is worth noticing that this value is one order of magnitude lower compared to the corresponding k_r evaluated at 298 K (Table 4). Such a difference can be attributed to the high zero-field splitting (zfs) between the three sublevels of the lowest triplet state that prevents a thermal equilibration of the sublevels at low temperatures; this is a well-known feature in cyclometalated Ir(III) complexes.[66,67] Accordingly, the first Arrhenius term of eq 1 (characterized by a low-frequency factor A_1 and a small activation-energy barrier ΔE_1) takes into account the zfs between the T_I and T_{III} substates and their thermal equilibration, which is obviously a temperature-dependent process. The estimated $T_I − T_{III}$ splitting is ~0.02 eV for both complexes (Table 6), in excellent agreement with previously reported values for similar Ir(III) compounds.[31,64,67]

Also the second Arrhenius terms used to fit the *cis*-3 and *trans*-3 intrinsic deactivation rates at high temperatures ($T >$ 250 K) are very similar, suggesting analogous photophysical processes for both complexes in the high-temperature regime. The rather low value of the frequency factor associated with the second process ($A_2 \approx$ (5−8) $\times 10^7$ s^{-1}) suggests that the corresponding calculated value of ΔE_2 (~0.12 eV) should be the energy separation between an upper-lying level that does not efficiently couple with S_0 and, therefore, does not drastically quench the emitting T_1 state.[7,64,65] Therefore, the different photophysical behavior of *cis*-3 and *trans*-3 is primarily

Table 6. Kinetic Parameters for Excited-State Decays Obtained from Temperature-Dependent Measurements in Oxygen-Free Propylene Glycol Solutions[a]

	k_0 (1×10^4 s^{-1})	A_1 (1×10^5 s^{-1})	ΔE_1 (eV)	A_2 (1×10^7 s^{-1})	ΔE_2 (eV)	B (1×10^5 s^{-1})	C (1×10^3 K)	T_g (K)
trans-3	5 ± 1	13 ± 3	0.015 ± 0.006	8.1 ± 0.6	0.108 ± 0.003	19.5 ± 0.5	8.3 ± 0.5	219.9 ± 0.4
cis-3	5 ± 3	7 ± 1	0.017 ± 0.004	5.0 ± 0.4	0.138 ± 0.004	1.8 ± 0.1	9 ± 2	211 ± 1

[a]An exhaustive discussion about the physical meaning of the fitting value is reported elsewhere.[64]

ascribable to solvation effects. In fact, the only parameter that significantly changes in the two fittings is B (see Table 6), which is proportional to solvent relaxation, that is, the ability of the dielectric medium to follow electronic and conformational changes of the excited-state complex relaxing to its T_1 minimum-energy geometry. B is one order of magnitude higher in the case of *trans*-3 (Table 6). As a consequence, prior to the glass-fluid transition of the solvent ($T_g \approx 216$ K) that occurs right above the melting point of propylene glycol ($T_m = 214$ K), the intrinsic deactivation rate constant of *trans*-3 is only twice as much that of *cis*-3, while at $T > T_g$, the k_{in} of the trans complex becomes 5 times higher than for the cis analogue.

The temperature-dependent measurements enable a rationalization of the differences observed between 298 and 77 K for *cis*-3 and *trans*-3. At low temperature, both complexes emit from a triplet state with a nonequilibrium solvation showing comparable energy and rate constants. As the temperature increases, solvent stabilization is more effective for the trans complex compared to that for the cis one, leading to a higher stabilization of T_1 and a smaller energy gap with S_0, which induces faster deactivation processes according to the energy-gap law.[68]

CONCLUSION

We have systematically investigated a family of photoactive cationic bis(heteroleptic) iridium(III) complexes bearing two cyclometalated carbene-based ligands. For the first time, cis and trans isomers of such complexes have been synthesized and their structural, electrochemical, and photophysical properties investigated. These compounds exhibit excellent reversibility of the electrochemical processes as well as high photoluminescence quantum yields, especially in the solid state. These combined properties hold great promise for the development of stable cationic iridium-based emitters for various applications such as light-emitting electrochemical cells, sensing, biolabeling, or protein staining. The detailed photophysical and theoretical studies here presented enable a full understanding of the nature and properties of the emissive excited states of the whole series and provide unprecedented insight on the different behavior of cis versus trans isomers.

ASSOCIATED CONTENT

Ⓢ Supporting Information

^{1}H NMR spectra (aromatic region) and high-resolution MS for all complexes. X-ray crystallographic data for the complexes *cis*-3 and *trans*-4 in CIF format and crystallographic data of the complexes. Illustration of HOMO and LUMO levels, visual comparison of calculated and experimental structures, calculated lowest triplet vertical excitations, and emission spectra. This material is available free of charge via the Internet at http://pubs.acs.org.

AUTHOR INFORMATION

Corresponding Authors
*E-mail: filippo.monti@isof.cnr.it. (F.M.)
*E-mail: nicola.armaroli@isof.cnr.it. (N.A.)
*E-mail: florian.kessler@siemens.com. (F.K.)

Present Address
⊥Siemens AG, Corporate Technology, CT RTC MAT IEC-DE, Günther-Scharowsky Strasse 1, D-91058 Erlangen, Germany.

Notes
The authors declare no competing financial interest.

REFERENCES

(1) Djurovich, P. I.; Thompson, M. E. In *Highly Efficient OLEDs with Phosphorescent Materials*; Wiley-VCH Verlag GmbH & Co. KGaA: 2008; p 131.
(2) Flamigni, L.; Barbieri, A.; Sabatini, C.; Ventura, B.; Barigelletti, F. *Top. Curr. Chem.* **2007**, *281*, 143.
(3) Nazeeruddin, M. K.; Grätzel, M. In *Photofunctional Transition Metal Complexes*; Yam, V. W., Ed.; Springer: Berlin Heidelberg, 2007; Vol. *123*, p 113.
(4) Kessler, F.; Watanabe, Y.; Sasabe, H.; Katagiri, H.; Nazeeruddin, M. K.; Gratzel, M.; Kido, J. *J. Mater. Chem. C* **2013**, *1*, 1070.
(5) Evans, R. C.; Douglas, P.; Winscom, C. J. *Coord. Chem. Rev.* **2006**, *250*, 2093.
(6) Thompson, M. E.; Djurovich, P. E.; Barlow, S.; Marder, S. In *Comprehensive Organometallic Chemistry III*; Crabtree, D., Michael, P., Mingos, R. H., Eds.; Elsevier: Oxford, U.K., 2007; p 101.
(7) Costa, R. D.; Orti, E.; Bolink, H. J.; Monti, F.; Accorsi, G.; Armaroli, N. *Angew. Chem., Int. Ed.* **2012**, *51*, 8178.
(8) Hu, T.; He, L.; Duan, L.; Qiu, Y. *J. Mater. Chem.* **2012**, *22*, 4206.
(9) Hasan, K.; Donato, L.; Shen, Y. L.; Slinker, J. D.; Zysman-Colman, E. *Dalton Trans.* **2014**, *43*, 13672.
(10) Sun, L. F.; Galan, A.; Ladouceur, S.; Slinker, J. D.; Zysman-Colman, E. *J. Mater. Chem.* **2011**, *21*, 18083.
(11) Curtin, P. N.; Tinker, L. L.; Burgess, C. M.; Cline, E. D.; Bernhard, S. *Inorg. Chem.* **2009**, *48*, 10498.
(12) McDaniel, N. D.; Coughlin, F. J.; Tinker, L. L.; Bernhard, S. *J. Am. Chem. Soc.* **2008**, *130*, 210.
(13) Di Marco, G.; Lanza, M.; Mamo, A.; Stefio, I.; Di Pietro, C.; Romeo, G.; Campagna, S. *Anal. Chem.* **1998**, *70*, 5019.
(14) Jia, J.; Fei, H.; Zhou, M. *Electrophoresis* **2012**, *33*, 1397.
(15) Wang, X.; Jia, J.; Huang, Z.; Zhou, M.; Fei, H. *Chem.—Eur. J.* **2011**, *17*, 8028.
(16) You, Y.; Cho, S.; Nam, W. *Inorg. Chem.* **2013**, *53*, 1804.
(17) Zhou, Y. Y.; Jia, J. L.; Li, W. F.; Fei, H.; Zhou, M. *Chem. Commun.* **2013**, *49*, 3230.
(18) Baranoff, E.; Curchod, B. F. E.; Frey, J.; Scopelliti, R.; Kessler, F.; Tavernelli, I.; Rothlisberger, U.; Grätzel, M.; Nazeeruddin, M. K. *Inorg. Chem.* **2011**, *51*, 215.
(19) Neve, F.; La Deda, M.; Puntoriero, F.; Campagna, S. *Inorg. Chim. Acta* **2006**, *359*, 1666.
(20) Lowry, M. S.; Bernhard, S. *Chem.—Eur. J.* **2006**, *12*, 7970.
(21) Yam, V. W. W.; Wong, K. M. C. *Chem. Commun.* **2011**, *47*, 11579.
(22) Garces, F. O.; King, K. A.; Watts, R. J. *Inorg. Chem.* **1988**, *27*, 3464.
(23) Fernandez-Hernandez, J. M.; Yang, C. H.; Beltran, J. I.; Lemaur, V.; Polo, F.; Frohlich, R.; Cornil, J.; De Cola, L. *J. Am. Chem. Soc.* **2011**, *133*, 10543.
(24) Zheng, Y. H.; Batsanov, A. S.; Bryce, M. R. *Inorg. Chem.* **2011**, *50*, 3354.
(25) Chien, C.-H.; Fujita, S.; Yamoto, S.; Hara, T.; Yamagata, T.; Watanabe, M.; Mashima, K. *Dalton Trans.* **2008**, 916.
(26) Tsuchiya, K.; Yagai, S.; Kitamura, A.; Karatsu, T.; Endo, K.; Mizukami, J.; Akiyama, S.; Yabe, M. *Eur. J. Inorg. Chem.* **2010**, *2010*, 926.
(27) Hitchcock, P. B.; Lappert, M. F.; Terreros, P. *J. Organomet. Chem.* **1982**, *239*, C26.
(28) Sajoto, T.; Djurovich, P. I.; Tamayo, A.; Yousufuddin, M.; Bau, R.; Thompson, M. E.; Holmes, R. J.; Forrest, S. R. *Inorg. Chem.* **2005**, *44*, 7992.

(29) Kessler, F.; Costa, R. D.; Di Censo, D.; Scopelliti, R.; Orti, E.; Bolink, H. J.; Meier, S.; Sarfert, W.; Gratzel, M.; Nazeeruddin, M. K.; Baranoff, E. *Dalton Trans.* **2012**, *41*, 180.

(30) Meier, S. B.; Sarfert, W.; Junquera-Hernandez, J. M.; Delgado, M.; Tordera, D.; Orti, E.; Bolink, H. J.; Kessler, F.; Scopelliti, R.; Gratzel, M.; Nazeeruddin, M. K.; Baranoff, E. *J. Mater. Chem. C* **2013**, *1*, 58.

(31) Monti, F.; Kessler, F.; Delgado, M.; Frey, J.; Bazzanini, F.; Accorsi, G.; Armaroli, N.; Bolink, H. J.; Orti, E.; Scopelliti, R.; Nazeeruddin, M. K.; Baranoff, E. *Inorg. Chem.* **2013**, *52*, 10292.

(32) Chang, C.-F.; Cheng, Y.-M.; Chi, Y.; Chiu, Y.-C.; Lin, C.-C.; Lee, G.-H.; Chou, P.-T.; Chen, C.-C.; Chang, C.-H.; Wu, C.-C. *Angew. Chem., Int. Ed.* **2008**, *47*, 4542.

(33) Harding, D. A. J.; Hope, E. G.; Singh, K.; Solan, G. A. *Organometallics* **2012**, *31*, 1518.

(34) Cao, Q.; Wang, J.; Tian, Z. S.; Xie, Z. F.; Bai, F. Q. *J. Comput. Chem.* **2012**, *33*, 1038.

(35) Stringer, B. D.; Quan, L. M.; Barnard, P. J.; Wilson, D. J. D.; Hogan, C. F. *Organometallics* **2014**, *33*, 4860.

(36) Duisenberg, A. J. M.; Kroon-Batenburg, L. M. J.; Schreurs, A. M. M. *J. Appl. Crystallogr.* **2003**, *36*, 220.

(37) Blessing, R. H. *Acta Crystallogr., Sect. A* **1995**, *51*, 33.

(38) Sheldrick, G. M. *Acta Crystallogr., Sect. A* **2008**, *64*, 112.

(39) Spek, A. L. *Acta Crystallogr. Sect. D: Biol. Crystallogr.* **2009**, *65*, 148.

(40) Frisch, M. J.; Trucks, G. W.; Schlegel, H. B.; Scuseria, G. E.; Robb, M. A.; Cheeseman, J. R.; Scalmani, G.; Barone, V.; Mennucci, B.; Petersson, G. A.; Nakatsuji, H.; Caricato, M.; Li, X.; Hratchian, H. P.; Izmaylov, A. F.; Bloino, J.; Zheng, G.; Sonnenberg, J. L.; Hada, M.; Ehara, M.; Toyota, K.; Fukuda, R.; Hasegawa, J.; Ishida, M.; Nakajima, T.; Honda, Y.; Kitao, O.; Nakai, H.; Vreven, T.; Montgomery Jr., J. A.; Peralta, J. E.; Ogliaro, F.; Bearpark, M. J.; Heyd, J.; Brothers, E. N.; Kudin, K. N.; Staroverov, V. N.; Kobayashi, R.; Normand, J.; Raghavachari, K.; Rendell, A. P.; Burant, J. C.; Iyengar, S. S.; Tomasi, J.; Cossi, M.; Rega, N.; Millam, N. J.; Klene, M.; Knox, J. E.; Cross, J. B.; Bakken, V.; Adamo, C.; Jaramillo, J.; Gomperts, R.; Stratmann, R. E.; Yazyev, O.; Austin, A. J.; Cammi, R.; Pomelli, C.; Ochterski, J. W.; Martin, R. L.; Morokuma, K.; Zakrzewski, V. G.; Voth, G. A.; Salvador, P.; Dannenberg, J. J.; Dapprich, S.; Daniels, A. D.; Farkas, O.; Foresman, J. B.; Ortiz, J. V.; Cioslowski, J.; Fox, D. J. *Gaussian 09*, Revision D.01; Gaussian, Inc.: Wallingford, CT, 2009.

(41) Adamo, C.; Barone, V. *J. Chem. Phys.* **1999**, *110*, 6158.

(42) Adamo, C.; Scuseria, G. E.; Barone, V. *J. Chem. Phys.* **1999**, *111*, 2889.

(43) Francl, M. M.; Pietro, W. J.; Hehre, W. J.; Binkley, J. S.; Gordon, M. S.; Defrees, D. J.; Pople, J. A. *J. Chem. Phys.* **1982**, *77*, 3654.

(44) Hay, P. J.; Wadt, W. R. *J. Chem. Phys.* **1985**, *82*, 299.

(45) Tomasi, J.; Persico, M. *Chem. Rev.* **1994**, *94*, 2027.

(46) Tomasi, J.; Mennucci, B.; Cammi, R. *Chem. Rev.* **2005**, *105*, 2999.

(47) Cramer, C. J.; Truhlar, D. G. In *Solvent Effects and Chemical Reactivity;* Tapia, O., Bertrán, J., Eds.; Springer: Netherlands, 2002; Vol. *17*, p 1.

(48) Stratmann, R. E.; Scuseria, G. E.; Frisch, M. J. *J. Chem. Phys.* **1998**, *109*, 8218.

(49) Casida, M. E.; Jamorski, C.; Casida, K. C.; Salahub, D. R. *J. Chem. Phys.* **1998**, *108*, 4439.

(50) Bauernschmitt, R.; Ahlrichs, R. *Chem. Phys. Lett.* **1996**, *256*, 454.

(51) Dennington, R.; Keith, T.; Millam, J. *GaussView*, Version 5; Semichem Inc.: Shawnee Mission, KS, 2009.

(52) Wurth, C.; Grabolle, M.; Pauli, J.; Spieles, M.; Resch-Genger, U. *Nat. Protoc.* **2013**, *8*, 1535.

(53) Nakamaru, K. *Bull. Chem. Soc. Jpn.* **1982**, *55*, 2697.

(54) deMello, J. C.; Wittmann, H. F.; Friend, R. H. *Adv. Mater.* **1997**, *9*, 230.

(55) Chu, Y.; Deng, H.; Cheng, J. P. *J. Org. Chem.* **2007**, *72*, 7790.

(56) Berding, J.; van Paridon, J. A.; van Rixel, V. H. S.; Bouwman, E. *Eur. J. Inorg. Chem.* **2011**, 2450.

(57) Slattery, J.; Thatcher Robert, J.; Shi, Q.; Douthwaite Richard, E. *Pure Appl. Chem.* **2010**, *82*, 1663.

(58) Takizawa, S. Y.; Shimada, K.; Sato, Y.; Murata, S. *Inorg. Chem.* **2014**, *53*, 2983.

(59) Humphrey, W.; Dalke, A.; Schulten, K. *J. Mol. Graphics Modell.* **1996**, *14*, 33.

(60) Monti, F.; Baschieri, A.; Gualandi, I.; Serrano-Perez, J. J.; Junquera-Hernandez, J. M.; Tonelli, D.; Mazzanti, A.; Muzzioli, S.; Stagni, S.; Roldan-Carmona, C.; Pertegas, A.; Bolink, H. J.; Orti, E.; Sambri, L.; Armaroli, N. *Inorg. Chem.* **2014**, *53*, 7709.

(61) Martin, R. L. *J. Chem. Phys.* **2003**, *118*, 4775.

(62) Bolink, H. J.; Cappelli, L.; Coronado, E.; Gratzel, M.; Orti, E.; Costa, R. D.; Viruela, P. M.; Nazeeruddin, M. K. *J. Am. Chem. Soc.* **2006**, *128*, 14786.

(63) Dragonetti, C.; Falciola, L.; Mussini, P.; Righetto, S.; Roberto, D.; Ugo, R.; Valore, A.; De Angelis, F.; Fantacci, S.; Sgamellotti, A.; Ramon, M.; Muccini, M. *Inorg. Chem.* **2007**, *46*, 8533.

(64) Costa, R. D.; Monti, F.; Accorsi, G.; Barbieri, A.; Bolink, H. J.; Orti, E.; Armaroli, N. *Inorg. Chem.* **2011**, *50*, 7229.

(65) Barigelletti, F.; Juris, A.; Balzani, V.; Belser, P.; Vonzelewsky, A. *J. Phys. Chem.* **1986**, *90*, 5190.

(66) Sajoto, T.; Djurovich, P. I.; Tamayo, A. B.; Oxgaard, J.; Goddard, W. A.; Thompson, M. E. *J. Am. Chem. Soc.* **2009**, *131*, 9813.

(67) Yersin, H.; Finkenzeller, W. J. In *Highly Efficient OLEDs with Phosphorescent Materials;* Wiley-VCH Verlag GmbH & Co. KGaA: 2008; p 1.

(68) Lakowicz, J. R. *Principles of Fluorescence Spectroscopy,* 3rd ed.; Springer: New York, 2006.